STM JOURNALS

Nano Trends:
A Journal of Nanotechnology and
Its Applications

ISSN: 0973-418X
Volume 28, Issue 1, 2026
January–April
DOI (Journal): 10.37591/NTs

https://journals.stmjournals.com/nts

Review NTs

Entropy Analysis of Unsteady MHD Bioconvective Nanofluid Between Parallel Disks Under Squeezing Motion and Multiple Slip Conditions

Sajid Khan[1], Yasir Abbasi[2], Iqrar Raza[3,*], Muhammad Awais[4]

Abstract

This research offers valuable insights for improving heat transfer and minimizing entropy generation in engineering systems that involve nanofluids and microorganisms. It investigates the unsteady squeezing bioconvection flow of a nanofluid between two parallel disks, with a focus on entropy generation, flow dynamics, heat transfer, and the concentration of both nanoparticles and microorganisms. The lower disk is stretched horizontally and subjected to suction, while the upper disk moves vertically, creating a squeezing effect. Temperature and concentration slip conditions are applied, and the problem is normalized using similarity transformations. To acquire numerical solutions, the bvp4c approach is utilized. The influence of various physical parameters particularly squeezing, magnetic, suction, Brownian motion, thermophoresis, and mass transfer parameters associated with the concentration of nanoparticles and microorganisms on fluid velocity, temperature, concentration profiles, and entropy generation is analyzed. Findings suggest that increasing the suction parameter reduces fluid velocity, while the squeezing and magnetic parameters enhance the velocity near the upper disk and hinders it near lower disk. Furthermore, an increase in the Brownian motion and thermophoresis parameters results in a reduction in nanoparticle concentration, whereas both parameters contribute to an elevation in the temperature profile. The study also highlights the impact of various factors such as Brinkman number and mass transfer parameter on entropy generation, Bejan number and overall system's efficiency.

Keywords: Entropy analysis, heat transfer enhancement, bioconvection, nanofluid, MHD, squeezing flow, slip condition, thermal efficiency

***Author for Correspondence**
Iqrar Raza
E-mail: iqrar.raza@yahoo.com

[1]Lecturer, Department of Mathematics, University of Wah, Wah Cantt, Pakistan
[2]Research Assistant, Department of Mechanical Engineering, University of Wah, Wah Cantt, Pakistan
[3]Researcher, Department of Mathematics and Statistics, International Islamic University Islamabad, Pakistan
[4]Assistant Professor, Researcher, Department of Mathematics and Statistics, International Islamic University Islamabad, Pakistan

Received Date: August 30, 2025
Accepted Date: February 17, 2026
Published Date: February 25, 2026

Citation: Iqrar Raza, Sajid Khan, Yasir Abbasi, Muhammad Awais. Entropy Analysis of Unsteady MHD Bioconvective Nanofluid Between Parallel Disks Under Squeezing Motion and Multiple Slip Conditions. Nano Trends: A Journal of Nanotechnology and Its Applications. 2026; 28(1): 17–39p.

INTRODUCTION

Squeezing flows between parallel disks have become a fascinating area of research due to their presence in various industrial applications, including food processing, printing technologies, material testing, coating processes and oil and gas industry. By applying a magnetic field in these flows helps mitigate unpredictable variations in lubrication viscosity caused by temperature fluctuations under extreme operating conditions. This phenomenon is crucial for improving efficiency in areas like power transmission, rotating machinery and geothermal energy systems. A deeper understanding of fluid transport and heat transfer in these setups is essential for driving advancements in industries such as chemical processing, electric power generation, and data storage technologies. Squeezing flows have been studied since the 19th century, with Stefan [1] conducting the foundational research on this topic. Misyura [2] analyzed a steady viscous flow generated by two rotating coaxial disks Von Kármán's [1] pioneering work on the single rotating disk [2] established the foundation for rotating flow analysis, and numerous subsequent investigations have built upon his formulation [2–6]. However, the two-disk configuration presents further complexities arising from geometric confinement and the unsteady nature of the squeezing motion. Batista [3] examined the steady and laminar flow between two parallel, hollow, co-rotating disks. The unsteady flow in this configuration has important industrial applications, prompting numerous researchers to explore the topic further. Thermal fluid flow because of rotating disks is studied by Tashtaush [4] and Khan [5]. Duwairi [6] has undertaken a study on the heat transfer properties associated with one directional squeezing flow occurring between two parallel disks. Khaled and Vafai [7] provided a numerical solution for the hydromagnetic squeezing flow occurring over a porous surface by considering the time variations.

Nanofluids consist of suspended nanoparticles with diameters smaller than 100 nm, utilized to enhance thermal conductivity. They have found extensive applications in solar thermal systems, wind turbines, refrigeration, hybrid vehicles and other renewable energy systems. Additionally, nanofluids are employed for automotive cooling, cancer therapy, dialysis, water purification and irrigation systems. The pioneering work in this field was carried out by Choi [8], whose research paved the way for further exploration of nanofluids by other researchers. Hashim et al. [9] conducted innovative research to develop and analyze a mathematical framework describing the behavior of a non-Newtonian Williamson fluid incorporating nanoparticles. Their research utilized the Rosseland approximation to describe the thermodynamic characteristics of the nanofluid and to exhibit the effects of nonlinear radiation. Benos et al. [10] investigated 2D MHD laminar transport process within a shallow cavity filled with a nanofluid. The study examined the impact of internal volumetric heat sources and examined an interfacial nanolayer near the solid particles. Their outcomes revealed that enhancing the concentration of carbon nanotube resulted in a reduction in fluid flow. Furthermore, various researchers have explored and discussed the distinctive behavior of nanofluid flow in diverse physical configurations, based on Buongiorno’s theory for example Kumar [11] investigated the flow and characteristics related to transfer of heat of magnetite nanofluid over a porous disk which is rotating while incorporating the effects of Arrhenius activation energy. Zaka et al. [12] developed an effective numerical approach to analyze the transport process of a third-grade nanofluid, incorporating gyrotactic microorganisms. Tausif et al. [13] examined the impact of multiple slip conditions on bioconvection in a nanofluid flow that contains nanoparticles and gyrotactic microorganisms. The flow and thermal transfer of hybrid nanofluids was studied by Xu [14].

Gyrotactic microorganisms exhibit a unique behavior known as gyrotaxis, where they align and swim along a specific axis, often influenced by rotational or directional forces within the fluid. Studying gyrotactic microorganisms in fluid flow is important because their movement significantly impacts bioconvection, which affects the overall behavior of the fluid, including heat and mass transfer. Understanding these microorganisms helps optimize processes in fields like biotechnology, wastewater treatment and environmental engineering, where fluid dynamics and microorganisms’ behavior play a crucial role in system’s efficiency. Qayyum et al. [15] analyzed the effects of radiation in a suspension containing nanoparticles and gyrotactic microorganisms on a rotating disk whose thickness is variable. Alshomrani [16] examined the significance of multiple slip conditions on cross nanofluid flow past a wedge in the existence of microorganisms.

Reducing entropy generation has become a key thermodynamic approach essential for the development of heating control systems. Bejan [17] is recognized for pioneering the concept of entropy generation. He concluded that minimizing entropy generation enhances a system’s thermodynamic efficiency, thereby improving the overall performance of thermal control systems. Studying entropy production in unsteady squeezing bioconvection flow of nanofluid between two disks arranged in parallel is essential for understanding and optimizing the thermodynamic efficiency of heat transfer systems. Entropy production quantifies the irreversibility of processes within the fluid, and minimizing it leads to improved energy utilization and reduced waste heat. In systems involving nanofluids, which exhibit enhanced thermal properties, analyzing entropy generation helps optimize heat transfer while minimizing losses due to viscous dissipation and other irreversible processes. This is particularly important in applications like cooling systems, microelectronics, and heat exchangers, where efficient flow control and stability are critical. The unsteady squeezing flow, under compressive forces between the disks, leads to variation in pressure and temperature that influence entropy generation, and understanding these effects allows for better design and operation of thermal management technologies. Notably, the principles of irreversibility in thermodynamics provide a robust framework for analysis than the first law, especially due to the first law's constraints on efficiency in thermal transfer engineering systems [18]. Recently, there has been a growing interest among researchers in applying the principles of irreversibility in the making of thermal systems. Aiboud and Saouli [19] discussed how these principles can be utilized to analyze MHD viscoelastic flow on a stretching surface. Similarly, Sahin and Yilbas [20] investigated the impact of entropy production in fluid flow within a channel formed by parallel plates. Rajvanshi et al. [21] explored the effects of entropy on squeezing flow from a porous. Their findings revealed that the total entropy production diminishes as the distance between the disks increases. Murshid et al. [22] studied the entropy production and performed a statistical analysis of the timely-varying squeezing flow of magnetohydrodynamic (MHD) hybrid nanofluid due to two rotating parallel plates, incorporating the effects of activation energy. Effects of entropy production in unsteady squeezing flow within a rotating channel that features a lower stretching permeable wall are analyzed by Butt and Asif [23]. Rashidi et al. [24] performed a parameter study and optimization of entropy generation in MHD flow over a rotating and stretching disk that changes with time. They employed an Artificial Neural Network along with a particle swarm optimization algorithm to analyze and enhance the system. Louati et al. [25] analyzed entropy production in magnetohydrodynamics (MHD) Casson fluid flow, incorporating the effects of Joule heating, using a non-similar numerical approach. The modified second-grade nanofluid flow comprising microorganisms is analyzed by Waqas et al. [26]. Entropy production in the radiative flow of tangent hyperbolic nanofluid is analyzed by Yong et al. [27], considering the effects of gyrotactic microorganisms and activation energy. Khan et al. [28] investigated entropy production in flow of bioconvection nanofluid through two stretchable rotating disks. Zuhra et al. [29] investigated the combined effects of gyrotactic microorganisms, nanoparticles, and second-grade nanofluid flow on heat transfer. They found that the temperature was increased as the thermophoresis parameter was raised. Research by Mehmood et al. [37] explored entropy behavior in a nanofluid on a rotating porous disk in forced flow. They observed that stronger forced flow, greater suction, and larger rotational Brinkman numbers all increase the average entropy generation number but decrease the average Bejan number. Adding nanoparticles, however, decreases average entropy generation while increasing the average Bejan number. Khan et al. [38] examined how entropy forms and heat distributes in a time-dependent squeezed nanofluid confined between parallel disks, where the bottom disk stretches horizontally and is subject to suction. The findings indicate that entropy generation grows with increases in the Brinkman parameter, magnetic parameter, and diffusion parameter. Meanwhile, the Bejan number follows a mixed trend, rising alongside the diffusion parameter yet falling as the Brinkman number climbs.

Building upon prior foundational studies, the present research provides a comprehensive investigation of entropy generation, fluid flow dynamics, heat transfer, and the distribution of nanoparticles and gyrotactic microorganisms. The governing equations are solved numerically using the MATLAB-based built-in bvp4c command. The influence of distinct parameters on different profiles is illustrated using graphs and tables.

Problem Description

Consider a two-dimensional, incompressible nanofluid flow between a pair of disks arranged in parallel and set apart by a time-dependent distance $h(t) = H\sqrt{1-at}$. The velocity components (u, v, w) are expressed in terms of cylindrical coordinates (r, θ, z). The lower disk which is kept at $z = 0$ has suction / injection w_0, is extended horizontally with velocity U_w. The upper disk is positioned at height

$h(t)$ which moves vertically upward and downward with velocity $w_h(t)$. The lower stretching disk has temperature T_w and nanoparticle concentration C_w and upper squeezing disk's temperature is T_h and nanoparticle concentration C_h. The lower and upper disks have gyrotactic microorganisms' distribution N_w and N_h, respectively. The magnetic field B is oriented perpendicular to the surface of the disks (Figure 1). In cylindrical coordinates, the equations that control the flow are [30]:

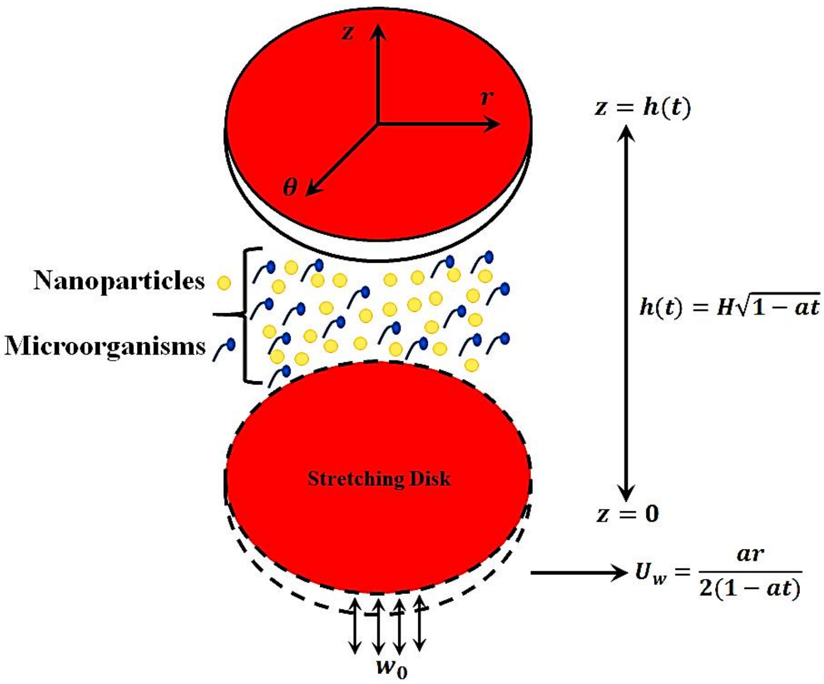

Figure 1. Fluid flow geometry and coordinate systems.

$$\frac{\partial u}{\partial r}+\frac{\partial w}{\partial z}+\frac{u}{r}=0, \tag{1}$$

$$\frac{\partial u}{\partial t}+u\frac{\partial u}{\partial r}+w\frac{\partial u}{\partial z}=-\frac{1}{\rho_f}\frac{\partial p}{\partial r}+\frac{\mu_f}{\rho_f}\left(\frac{\partial^2 u}{\partial r^2}-\frac{u}{r^2}+\frac{\partial^2 u}{\partial z^2}+\frac{1}{r}\frac{\partial u}{\partial r}\right)-\frac{\sigma_e B^2}{\rho_f}u, \tag{2}$$

$$\frac{\partial w}{\partial t}+u\frac{\partial w}{\partial r}+w\frac{\partial w}{\partial z}=-\frac{1}{\rho_f}\frac{\partial p}{\partial z}+\frac{\mu_f}{\rho_f}\left(\frac{\partial^2 w}{\partial r^2}+\frac{\partial^2 w}{\partial z^2}+\frac{1}{r}\frac{\partial w}{\partial r}\right), \tag{3}$$

$$\frac{\partial T}{\partial t}+u\frac{\partial T}{\partial r}+w\frac{\partial T}{\partial z}=\alpha_f\left(\frac{\partial^2 T}{\partial r^2}+\frac{1}{r}\frac{\partial T}{\partial r}+\frac{\partial^2 T}{\partial z^2}\right)+\tau D_B\left(\frac{\partial T}{\partial r}\frac{\partial C}{\partial r}+\frac{\partial T}{\partial z}\frac{\partial C}{\partial z}\right)$$
$$+\tau\left(\frac{D_T}{T_m}\right)\left(\left(\frac{\partial T}{\partial r}\right)^2+\left(\frac{\partial T}{\partial z}\right)^2\right), \tag{4}$$

$$\frac{\partial C}{\partial t}+u\frac{\partial C}{\partial r}+w\frac{\partial C}{\partial z}=D_B\left(\frac{\partial^2 C}{\partial r^2}+\frac{1}{r}\frac{\partial C}{\partial r}+\frac{\partial^2 C}{\partial z^2}\right)+\left(\frac{D_T}{T_m}\right)\left(\frac{\partial^2 T}{\partial r^2}+\frac{1}{r}\frac{\partial T}{\partial r}+\frac{\partial^2 T}{\partial z^2}\right), \tag{5}$$

$$\frac{\partial n}{\partial t}+u\frac{\partial n}{\partial r}+w\frac{\partial n}{\partial z}+\frac{\partial (n\,\hat{w})}{\partial z}=D_n\left(\frac{\partial^2 n}{\partial r^2}+\frac{1}{r}\frac{\partial n}{\partial r}+\frac{\partial^2 n}{\partial z^2}\right), \tag{6}$$

and the boundary conditions are [23, 30]

$$\begin{aligned}
&u=0,\quad w=\frac{dh}{dt},\quad T=T_h-\delta_T\frac{\partial T}{\partial z},\qquad C=C_h-\delta_C\frac{\partial C}{\partial z},\ n=N_h,\qquad at\quad z=h(t),\\
&u=U_w=\frac{ar}{2(1-at)},\ w=-w_0,\ T=T_w+\delta_T\frac{\partial T}{\partial z},\ C=C_w+\delta_C\frac{\partial C}{\partial z},\ n=N_w,\quad at\quad z=0.
\end{aligned} \tag{7}$$

Here $h(t)=H\sqrt{1-at}$ illustrates the separation of disks and both a and H are constants. u and w are the components of velocity in the directions of r and z , respectively. ρ_f represents the density of nanofluid, μ_f is used for dynamic nanofluid's viscosity, p is representing pressure, nanoparticles' concentration is represented by C, nanofluid's thermal diffusivity is given by α_f , D_B represents the Brownian motion coefficient, D_T indicates the thermophoresis diffusion coefficient and T_m represents the fluid's mean temperature. N_w and N_h are constants related to distribution of gyrotactic microorganisms. Moreover, w_0 represents the suction or injection velocity of lower disk, δ_T and δ_C are used for thermal and concentration slip parameters, respectively. The quantity τ is the ratio of the effective thermal capacity of the nanoparticle material to the base fluid. Consequently, τ will vary depending on the particular fluid and nanoparticle's material employed. Following Hashmi and Pradhan [31, 32], the similarity variables are presented as:

$$\begin{aligned}
&u=\frac{ar}{2(1-at)}f'(\eta),\quad w=-\frac{aH}{\sqrt{1-at}}f(\eta),\quad T=(T_w-T_h)\theta(\eta)+T_h,\\
&C=(C_w-C_h)\,\varphi(\eta)+C_h,\ \ n=(N_w-N_h)s(\eta)+N_h,\ \ B(t)=\frac{B_0}{\sqrt{1-at}},\\
&\eta=\frac{z}{H\sqrt{1-at}}.
\end{aligned} \tag{8}$$

Equation (1) will remain true and Eqs. (2–6) are transformed as follows when aforementioned similarity transformations are applied.

$$f''''-S_q(\eta f'''-2ff'''+3f'')-2M^2S_q=0, \tag{9}$$

$$\theta'' + P_r S_q (2f\theta' - \eta\theta') + p_r N_b \theta' \varphi' + p_r N_b \theta'^2 = 0, \tag{10}$$

$$\varphi'' + L_e S_q (2f\varphi' - \eta\varphi') + \left(\frac{N_t}{N_b}\right)\theta'' = 0, \tag{11}$$

$$s'' + S_c S_q (2fs' - \eta s') - p_{eb}(s - N_d)\varphi'' - p_{eb}\varphi' s' = 0, \tag{12}$$

where S_q represents squeezing parameter, M symbolizes the magnetic parameter, P_r is used for Prandtl number, N_b denotes the Brownian motion coefficient, L_e symbolizes the Lewis number, N_t is thermophoresis coefficient, Pe_b is the Peclet number, the symbol S_c is used for Schmidt number and N_d is the constant associated with microorganism's distribution, expressed by:

$$S_q = \frac{aH^2}{2\upsilon_f},\ M = \sqrt{\frac{\sigma_e B_0^{\ 2}}{a\rho_f}}, N_b = \frac{\tau D_B (C_w - C_h)}{\upsilon_f},\ N_t = \frac{\tau D_T (T_w - T_h)}{\upsilon_f T_m},$$
$$L_e = \frac{\upsilon_f}{D_B},\ Pe_b = \frac{bw_c}{D_n},\ P_r = \frac{\upsilon_f}{\alpha_f},\ S_c = \frac{\upsilon_f}{D_n},\ N_d = \frac{N_h}{N_w - N_h}. \tag{13}$$

The following form of the boundary conditions (7) is obtained after the application of transformations:

$$f(0) = S,\ f'(0) = 1,\quad \theta(0) - \gamma_1\theta'(0) = 1,\quad \varphi(0) - \gamma_2\varphi'(0) = 1,\ s(0) = 1,$$
$$f(1) = \frac{1}{2},\quad f'(1) = 0,\quad \theta(1) + \gamma_1\theta'(1) = 0,\quad \varphi(1) + \gamma_2\varphi'(1) = 0,\ s(1) = 0, \tag{14}$$

where S is suction / injection parameter, γ_1 is representing thermal slip parameter and γ_2 is used for concentration slip parameter, given by:

$$S = \frac{w_0\sqrt{1-at}}{aH},\quad \gamma_1 = \frac{\delta_T}{H\sqrt{1-at}},\quad \gamma_2 = \frac{\delta_C}{H\sqrt{1-at}}. \tag{15}$$

Fluid suction at the lower disk is indicated by $S > 0$, whereas $S < 0$ corresponds to the blowing of the fluid. Zero values of both N_b and N_t represent the case when effects of both Brownian motion and thermophoresis are minimal and that kind of fluid is an ordinary fluid. The skin friction coefficient, Nusselt number and Sherwood number are demonstrated mathematically as follows:

$$C_{fr} = \frac{\tau_w}{\rho_f\left(\frac{-aH}{2\sqrt{1-at}}\right)^2},\quad Nu = \frac{Hq_w}{k_f(T_w - T_h)},\quad Sh = \frac{Hj_w}{D_B(C_w - C_h)}, \tag{16}$$

where τ_w denotes shear stress, q_w represents heat flux of the wall and j_w is the mass flux of the wall, given as:

$$\tau_w = \mu_f\left(\frac{\partial u}{\partial z} + \frac{\partial u}{\partial r}\right), \quad q_w = -k_f\left(\frac{\partial T}{\partial z}\right), \quad j_w = -D_B\left(\frac{\partial C}{\partial z}\right). \tag{17}$$

By using the similarity transformations (7), we have:

$$H^2 \frac{\mathrm{Re}_r}{r^2} C_{fr} = f''(\eta), \quad Nur = \sqrt{1-at}\; Nu = -\theta'(\eta), \quad Shr = -\varphi'(\eta), \tag{18}$$

where,

$$\mathrm{Re}_r = \frac{raH\sqrt{1-at}}{2\upsilon}$$

ENTROPY ANALYSIS

The entropy production for a viscous, incompressible fluid is calculated using:

$$S_G = \frac{k_f}{T_h^2}\left(\frac{\partial T}{\partial z}\right)^2 + \frac{\mu_f}{T_h}\left(\frac{\partial u}{\partial z}\right)^2 + \frac{\sigma_e}{T_h}B^2u^2 + \frac{RD}{C_h}\left(\frac{\partial C}{\partial z}\right)^2 + \frac{RD}{T_h}\left(\frac{\partial C}{\partial z}\frac{\partial T}{\partial z}\right) + \frac{RD}{N_h}\left(\frac{\partial n}{\partial z}\right)^2 + \frac{RD}{T_h}\left(\frac{\partial n}{\partial z}\frac{\partial T}{\partial z}\right), \tag{19}$$

where D stands for diffusivity and R for the ideal gas constant. The characteristic entropy rate is given by:

$$S_{G0} = \frac{k_f(\Delta T)^2}{T_h^2 h^2}. \tag{20}$$

By using transformations (7), the entropy production number $N_s = \frac{S_G}{S_{G0}}$ will be expressed as:

$$N_s = \theta'^2 + \frac{Br}{\Omega_T}\left(f''^2 + 2M^2 S_q f'^2\right) + \frac{\lambda}{\Omega_T}\left(\frac{\Omega_C}{\Omega_T}\varphi'^2 + \theta'\varphi'\right) + \frac{\varepsilon}{\Omega_T}\left(\frac{1}{N_d\Omega_T}s'^2 + \theta' s'\right), \tag{21}$$

where,

$$Br = \frac{\mu_f U_w^2}{k_f \Delta T}, \quad \Omega_T = \frac{(T_w - T_h)}{T_h}, \quad \Omega_c = \frac{(C_w - C_h)}{C_h},$$
$$\lambda = \frac{RD}{k_f}(C_w - C_h), \quad \varepsilon = \frac{RD}{k_f}(N_w - N_h), \tag{22}$$

are the Brinkman number, thermal and concentration ratio parameter, mass transfer parameters of nanoparticles and microorganisms' concentration, respectively. Bejan number is expressed through the following form:

$$Be = \frac{The\ \ production\ \ of\ \ entropy\ \ as\ \ a\ \ result\ \ of\ \ heat\ \ and\ \ mass\ transfer}{Overall\ \ production\ of\ \ \ entropy}, \tag{23}$$

$$Be = \frac{\theta'^2 + \frac{\lambda}{\Omega_T}\left(\frac{\Omega_C}{\Omega_T}\varphi'^2 + \theta'\varphi'\right) + \frac{\varepsilon}{\Omega_T}\left(\frac{1}{N_d\Omega_T}s'^2 + \theta' s'\right)}{\theta'^2 + \frac{Br}{\Omega_T}\left(f''^2 + 2M^2 S_q f'^2\right) + \frac{\lambda}{\Omega_T}\left(\frac{\Omega_C}{\Omega_T}\varphi'^2 + \theta'\varphi'\right) + \frac{\varepsilon}{\Omega_T}\left(\frac{1}{N_d\Omega_T}s'^2 + \theta' s'\right)}. \tag{24}$$

Range of Bejan number is $[0,1]$. Heat distribution is the primary cause of the entropy generation for $0.5 < Be \le 1$, whereas the primary source of entropy creation in $0 \le Be < 0.5$ is friction with the fluid. $Be = 0.5$ corresponds to equal contribution of thermal distribution and friction in the production of entropy.

PROBLEM SOLUTION

MATLAB built in package bvp4c [33] is adopted to solve the system of ODEs described by Eqs. (9–12) as well as boundary conditions specified by Eq. (14). The domain, based on the boundary conditions, is defined as $\eta\, \varepsilon [0,1]$.

$$\begin{aligned}
&\eta = x,\\
&f = y_1,\\
&f' = y_2,\\
&f'' = y_3,\\
&f''' = y_4,\\
&y_4' = S_q(xy_4 - 2y_1y_4 + 3y_3 + 2M^2S_qy_3),\\
&\theta = y_5,\\
&\theta' = y_6,\\
&\varphi = y_7,\\
&\varphi' = y_8,\\
&y_6' = -P_rS_q(2y_1y_6 - xy_6) - P_rN_by_6y_8 - P_rN_ty_6^2,\\
&y_8' = -L_eS_q(2y_1y_8 - xy_8) - \left(\frac{N_t}{N_b}\right)y_6',\\
&y_{10}' = -S_cS_q(2y_1y_{10} - xy_{10}) + Pe_by_9y_8' + Pe_bN_dy_8' + Pe_by_8y_{10}.
\end{aligned} \tag{25}$$

After applying the transformations, the boundary conditions are reformulated as:

$$\begin{aligned}
&y_1(0) = S,\ y_2(0) = 1,\ y_5(0) - \gamma_1y_6(0) = 1,\ y_7(0) - \gamma_2y_8(0) = 1,\ y_9(0) = 1,\\
&y_1(1) = \frac{1}{2},\ y_2(1) = 0,\ y_5(1) + \gamma_1y_6(1) = 0,\ y_7(1) + \gamma_2y_8(1) = 0,\ y_9(1) = 0.
\end{aligned} \tag{26}$$

The entropy equation and Bejan number are transformed into the following form:

$$N_s = {y_6}^2 + \frac{Br}{\Omega_T}({y_3}^2 + 2M^2 S_q {y_2}^2) + \frac{\lambda}{\Omega_T}\left(\frac{\Omega_C}{\Omega_T}{y_8}^2 + y_6 y_8\right) + \frac{\varepsilon}{\Omega_T}\left(\frac{1}{N_d \Omega_T}{y_{10}}^2 + y_{10} y_6\right), \tag{27}$$

$$Be = \frac{{y_6}^2 + \frac{\lambda}{\Omega_T}\left(\frac{\Omega_C}{\Omega_T}{y_8}^2 + y_6 y_8\right) + \frac{\varepsilon}{\Omega_T}\left(\frac{1}{N_d \Omega_T}{y_{10}}^2 + y_{10} y_6\right)}{{y_6}^2 + \frac{Br}{\Omega_T}({y_3}^2 + 2M^2 S_q {y_2}^2) + \frac{\lambda}{\Omega_T}\left(\frac{\Omega_C}{\Omega_T}{y_8}^2 + y_6 y_8\right) + \frac{\varepsilon}{\Omega_T}\left(\frac{1}{N_d \Omega_T}{y_{10}}^2 + y_{10} y_6\right)}. \tag{28}$$

RESULTS AND DISCUSSION

Equations (9–12) together with the boundary conditions (14) and Eqs. (21) and (24) are numerically solved using bvp4c. The results are presented and briefly discussed through tables and graphs. Additionally, the influence of physical parameters on flow velocity, temperature distribution, concentration profiles and entropy production are analyzed. Figure 2 shows how the fluid velocity curve f' changes with changing squeezing parameter S_q. As the squeezing parameter rises, the velocity of the fluid drops close to lower disk, while near upper disk, the velocity escalates with S_q. When the upper disk compresses the fluid through its squeezing motion, it creates a downward pressure that resists the flow near the lower disk. As a result, this opposing force causes a significant decrease in velocity near the lower disk. On the other hand, due to increased squeezing effect upper plate imparts more energy to the surrounding fluid as a result velocity is increased near upper disk. Figure 3 demonstrates the impact of the magnetic parameter M on f'. As the magnetic parameter increases, the fluid velocity near the lower disk decreases, while it increases close to upper disk. As the strength of the magnetic field grows, the Lorentz force generated acts as a resistance to the fluid's movement, causing a decrease in velocity throughout most of the flow region. However, near the upper disk, the squeezing motion of the disk plays a more significant role, transferring momentum to the fluid. This results in a noticeable rise in velocity close to the upper boundary. Figure 4 illustrates the impact of suction parameter S on f'. A suction parameter value of zero indicates no suction, resulting in a curve that is not parabolic. As S grows, the velocity of the fluid is diminished throughout the entire region between the parallel disks. With stronger suction, the fluid is drawn downward, leading to a reduction in velocity across all layers, causing an overall decline in the velocity of the fluid between the disks.

Figure 5 displays the effect of the Brownian motion parameter N_b on the thermal field for multiple values of γ_1. As N_b elevates, the temperature profile also rises. In Brownian motion, the rapid collision between particles leads to an increase in their movement, which in turn raises the temperature field. Additionally, for higher values of γ_1, the thermal curves display a linear trend. Figure 6 illustrates the effect of thermophoresis parameter N_t on the thermal profile for multiple γ_1 values. It is evident from the figure that particles tend to move from regions of higher temperature to low temperature. Consequently, thermal field is amplified with N_t. Figure 7 demonstrates the Brownian motion coefficient's effect on $\varphi(\eta)$ (nanoparticles concentration) for three different values of γ_2. A growth in N_b values cause decline in the graph of φ. As Brownian motion coefficient intensifies, the particles experience more collisions, causing them to spread out more evenly. This increased diffusion effect results in the redistribution of particles, which lowers the concentration of fluid in any specific region. Essentially, the particles become more dispersed, reducing the overall concentration in the fluid. In Figure 8, influence of thermophoresis parameter N_t on φ for multiple values of γ_2 is presented. After analyzing three cases of the concentration slip parameter γ_2, we found that increasing its values result in a reduction of the concentration field. Higher slip values increase the rate at which particles are displaced from the surface, reducing their local concentration.

Figure 9 shows how the gyrotactic microorganisms' concentration profile $s(\eta)$ changes with the squeezing parameter S_q. As the squeezing number S_q increases, the flow gets more compressed, which spreads the gyrotactic microorganisms more evenly. This stronger squeezing pushes the microorganisms away from the lower plate and reduces their buildup in one area. The increased movement in the flow makes it harder for the microorganisms to stay concentrated, leading to an overall decrease in their concentration. Figure 10 illustrates how the profile s is affected by the Schmidt number S_c. With growth of S_c, the profile s decreases. The decrease is because higher S_c values indicate that the mass diffusivity is low as compared to the momentum diffusivity. This results in reduced mixing and slower spreading of microorganisms throughout the fluid. As a consequence, the microorganisms are less able to diffuse, leading to a lower concentration profile. Figure 11 highlights the impact of the bioconvection Peclet number Pe_b on the profile $s(\eta)$. A decrease in the s is observed with surge in Pe_b. This occurs since Peclet number has inverse relation with diffusivity of microorganisms, leading to a reduction in their density. Figure 12 demonstrates the bioconvection Lewis number's (L_e) impact on the profile $s(\eta)$ of gyrotactic microorganisms. A decrease in s is observed as L_e increases. This behavior is attributed to the reduced diffusivity of microorganisms.

Figure 13 depicts the impact of the Brinkman number Br on entropy production, showing that entropy production rises with higher Brinkman number. This surge is mainly attributed to the friction of the fluid, which amplifies entropy production. Physically, higher Br indicates that maximum amount of mechanical energy is transformed to heat due to internal friction of the fluid, leading to a decrease in the efficiency of thermal system. Figure 14 reveals the influence of mass transfer parameter λ on entropy production. As λ increases, entropy production steadily increases. Figure 15 investigates how the microorganisms' mass transfer parameter ε influences entropy production. Enhancement in ε leads to a corresponding rise in entropy production. This is because higher diffusivity allows the microorganisms to spread more rapidly, enhancing their interaction with the surrounding fluid. As a result, maximum amount of mechanical energy is transformed to heat energy, thereby increasing entropy. Figure 16 examines the effect of Br on the Bejan number Be. As Br is enhanced, Be is declined. This occurs because Br is the ratio of viscous dissipation to thermal conduction. As Br is increased, the effect of viscous dissipation becomes more significant. Thus, higher viscous dissipation (with a higher Brinkman number) leads to a lower efficiency of thermal energy transport, resulting in a reduced Bejan number. From Figure 17, with increase in mass transfer parameter λ, the Bejan number rises. As the concentration of nanoparticles increases, the diffusion of particles in the fluid improves, which enhances the overall thermal conductivity, which leads to more effective heat distribution that results in enhancement in the Be. Figure 18 illustrates the impact of the mass transfer parameter of microorganism concentration ε on Be. As ε escalates, Be also rises. Increase in ε improves the diffusion process. As higher microorganism concentration promotes better heat transfer, as a result Bejan number is boosted.

Table 1 presents the numerical values of skin friction coefficient at upper disk against different values of S_q, S and M by keeping lower disk fixed. The results show excellent agreement with previously published work, thereby validating the accuracy and effectiveness of the numerical approach adopted in this study. Table 2 is created to analyze the behavior of the skin friction coefficient at lower and upper disks for various values of the magnetic parameter M, squeezing parameter S_q, and suction parameter S. It is observed that elevation in the squeezing and magnetic parameters cause fall in shear stress at both disks. In contrast, the suction parameter reduces shear stress at lower disk but increases it at upper disk. Table 3 is designed to show the Nusselt number in relation to various parameters. The rate of heat transmission at the lower disk falls as the Prandtl number increases, whereas it increases at the top disk. Heat transfer rate ascends at the lower disk when the suction parameter values rise, but it decreases at the top disk. At both disks, the heat transfer rate decreases as γ_1 is amplified. The influence of various parameters on the Sherwood number Sh_r is displayed in Table 4. It has been observed that the Prandtl and Lewis numbers have similar impact on Sh_r, i.e., with rise in both parameters, the Sherwood number also shows surge at the lower disk and diminishes at the upper disk. Additionally, concentration slip parameter values on the Sherwood number Sh_r show a decreasing trend.

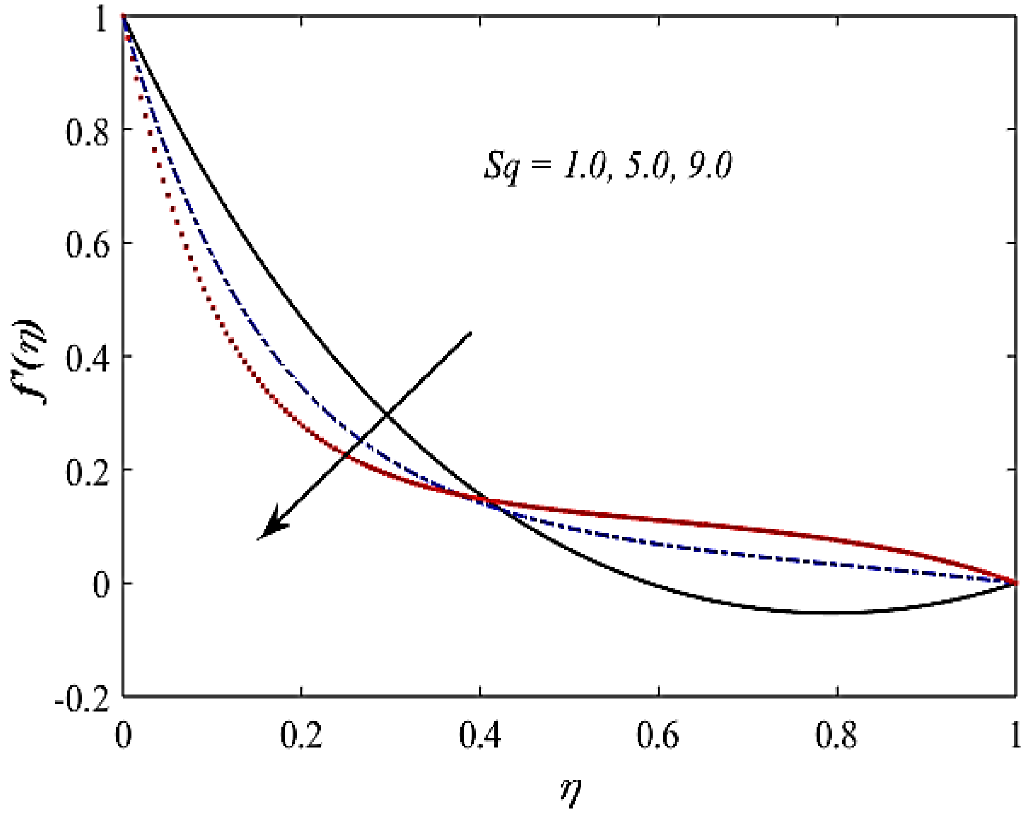

Figure 2. $f'(\eta)$ against η for different S_q values. Here:

$M=0.5,\ P_r=1.0,\ N_b=N_t=0.3,\ L_e=0.2,\ \ S=0.3, \gamma_1=0.5,\ \ \gamma_2=0.5,\ \ S_c=1.0,\ \ Pe_b=1.0,\ \ \ N_d=0.5$

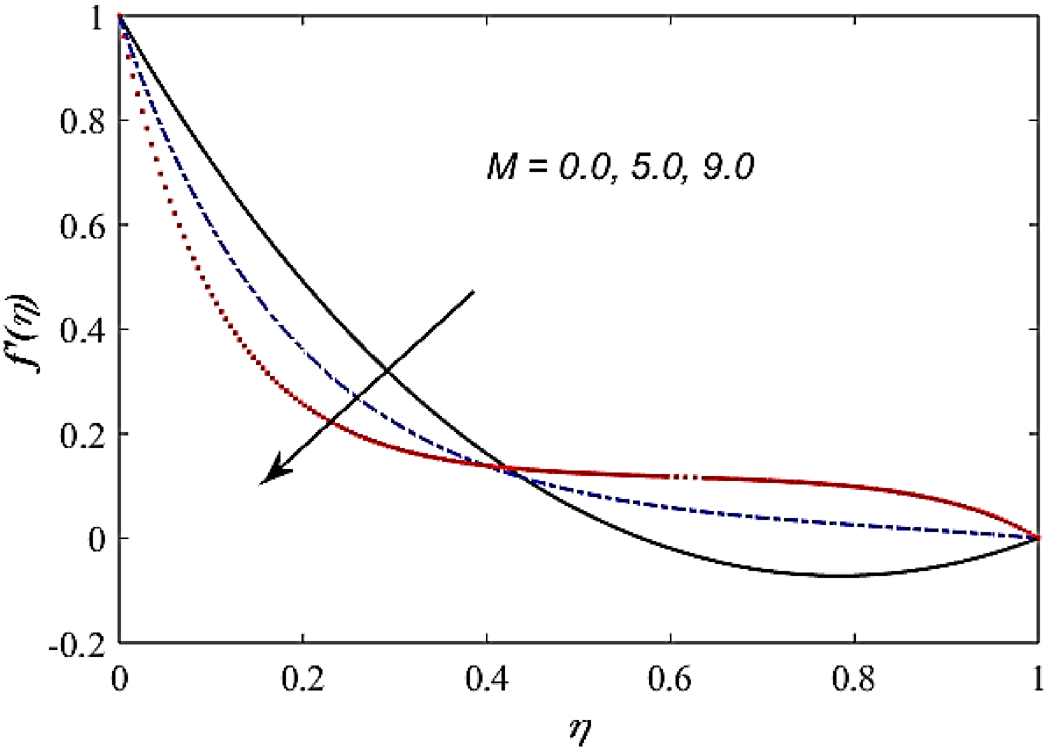

Figure 3. Velocity profile against η for different M values. Here:
$S_q = 0.5,\ P_r = 1.0,\ N_b = N_t = 0.3,\ L_e = 0.2,\ S = 0.3, \gamma_1 = 0.5,\ \ \gamma_2 = 0.5,\ \ S_c = 1.0,\ \ Pe_b = 1.0,\ \ N_d = 0.5$

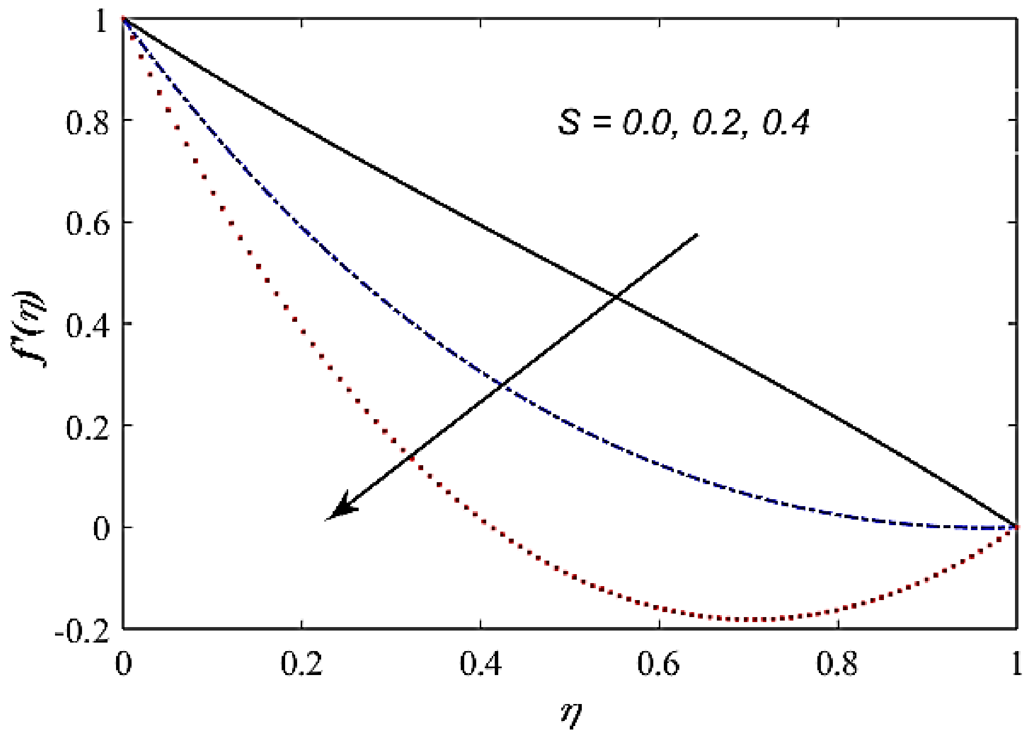

Figure 4. Impact of S upon $f'(\eta)$. Here:
$M = 0.5,\ P_r = 1.0,\ N_b = N_t = 0.3,\ L_e = 0.2,\ S_q = 0.5, \gamma_1 = 0.5,\ \ \gamma_2 = 0.5,\ \ S_c = 1.0,\ \ Pe_b = 1.0,\ \ N_d = 0.5$

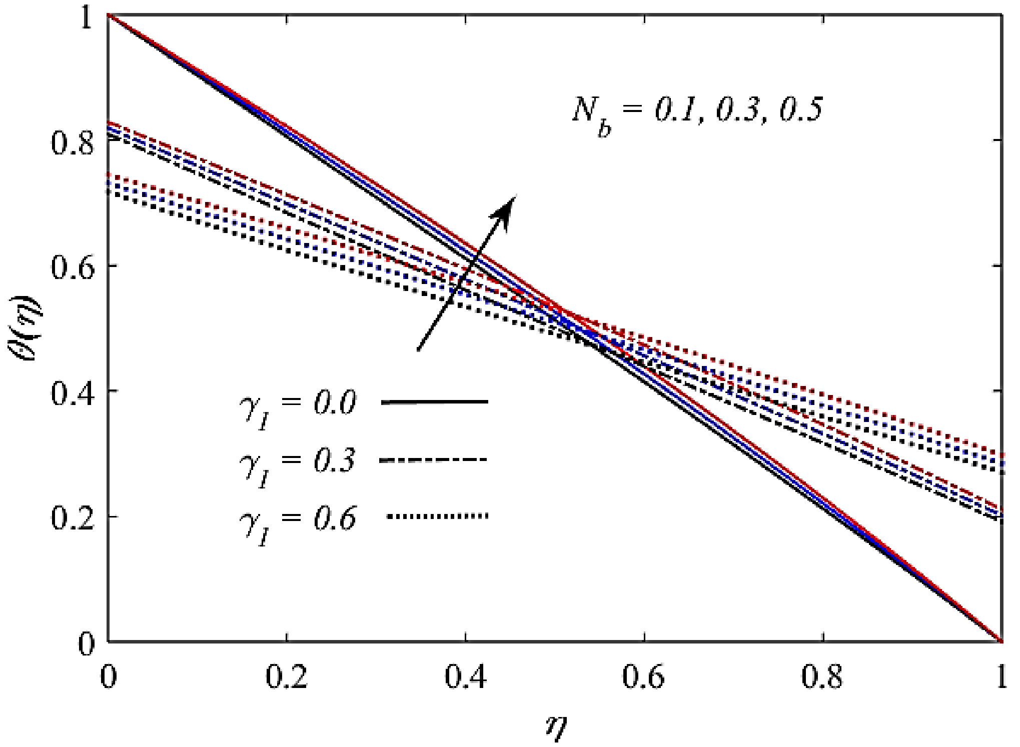

Figure 5. $\theta(\eta)$ against η for different γ_1 and N_b values. Here:
$M = 0.5,\ P_r = 1.0,\ N_t = 0.3,\ L_e = 0.2,\ S_q = 0.5,\ S = 0.3,\ \gamma_2 = 0.5,\ S_c = 1.0, Pe_b = 1.0,\ N_d = 0.5$

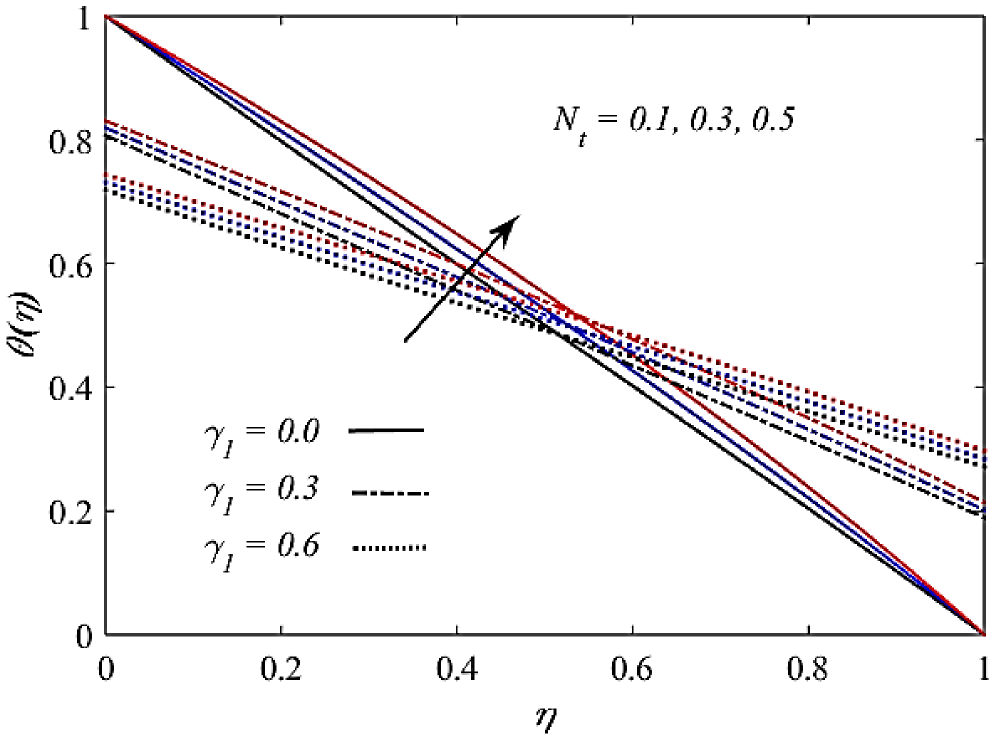

Figure 6. Temperature profile against η for different γ_1 and N_t values. Here:
$M = 0.5,\ P_r = 1.0,\ N_b = 0.3,\ L_e = 0.2,\ S_q = 0.5,\ S = 0.3,\ \gamma_2 = 0.5,\ S_c = 1.0, Pe_b = 1.0, N_d = 0.5$

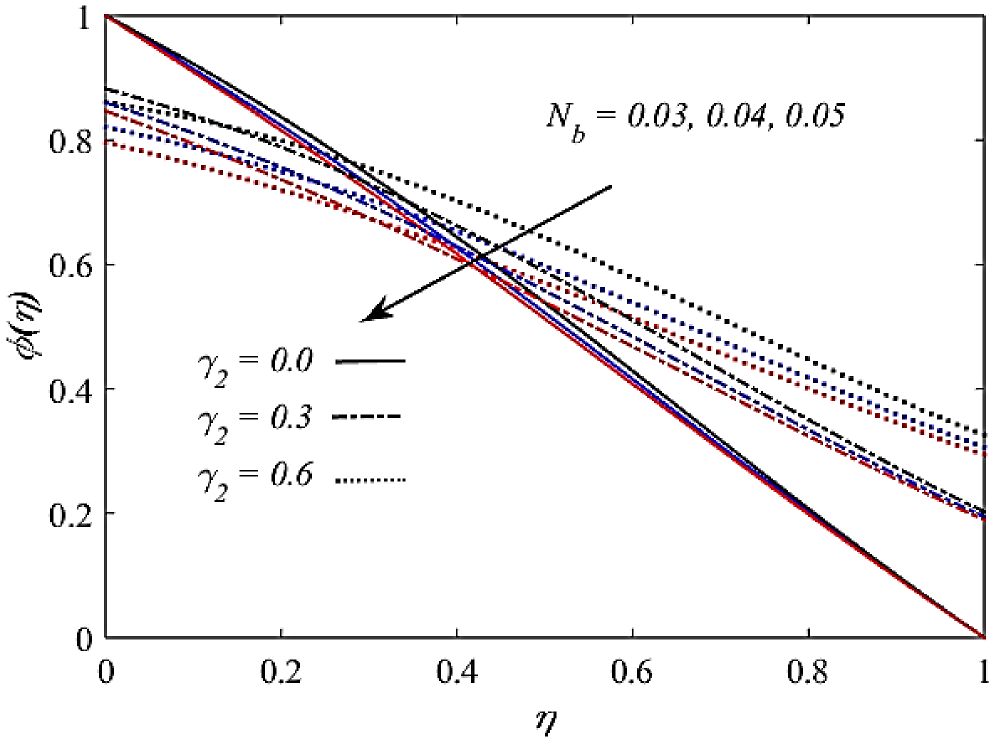

Figure 7. $\varphi(\eta)$ against η for different γ_2 and N_b values. Here:
$M = 0.5,\ P_r = 1.0,\ N_t = 0.3,\ L_e = 0.2,\ S_q = 0.5,\ S = 0.3,\ \gamma_1 = 0.5,\ S_c = 1.0, Pe_b = 1.0, N_d = 0.5$

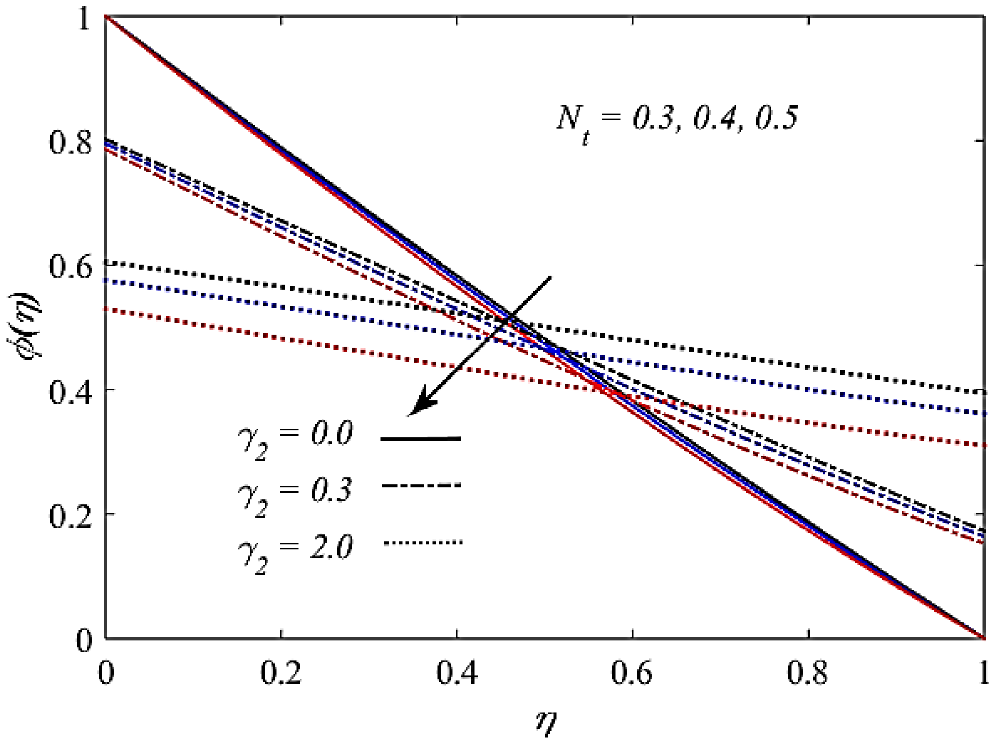

Figure 8. Concentration profile against η for different γ_2 and N_t values. Here:
$M = 0.5,\ P_r = 1.0,\ N_b = 0.3,\ L_e = 0.2,\ S_q = 0.5,\ S = 0.3,\ \gamma_2 = 0.5,\ S_c = 1.0, Pe_b = 1.0, N_d = 0.5$

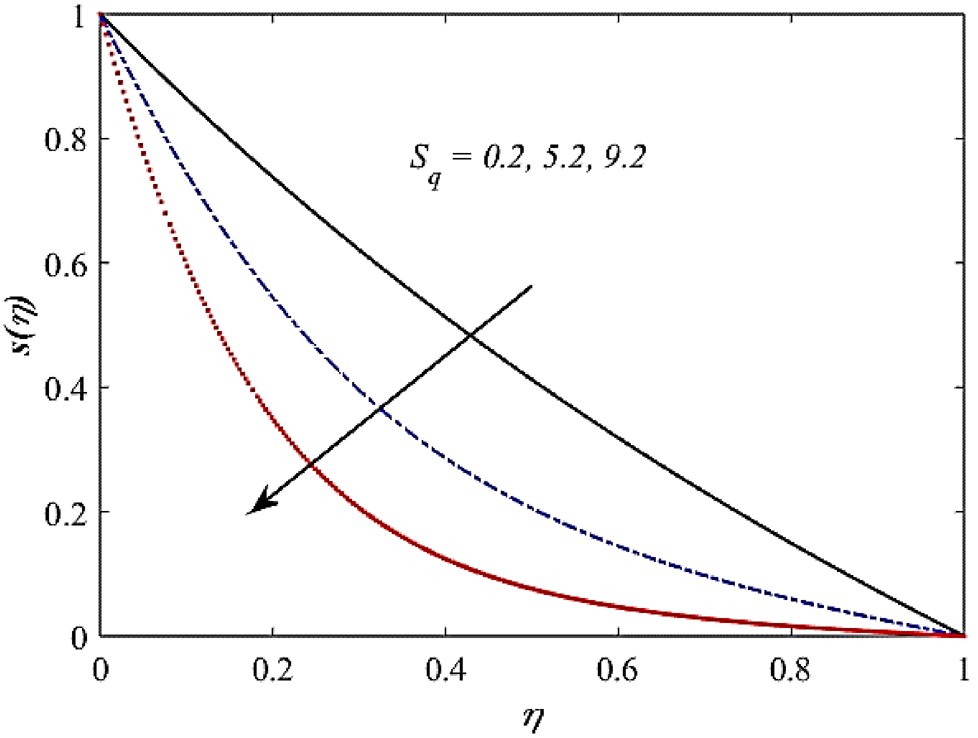

Figure 9. $s(\eta)$ against η for different S_q values. Here:
$N_b = 0.3, P_r = 1.0,\ L_e = 0.2,\ S = 0.3, N_t = 0.3,\ \gamma_2 = 0.5,\ \gamma_1 = 0.5, S_c = 1.0, Pe_b = 1.0, N_d = 0.5, M = 0.5$

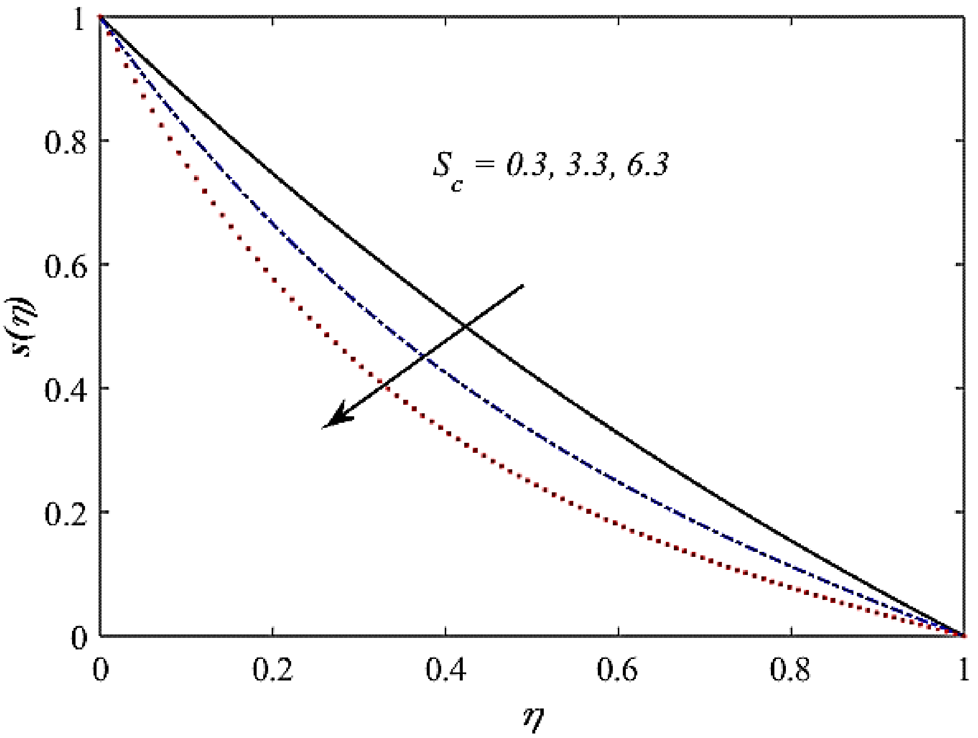

Figure 10. $s(\eta)$ against η for different S_c values. Here:
$P_r = 1.0,\ N_t = 0.3,\ N_b = 0.3, M = 0.5,\ L_e = 0.2,\ S_q = 0.5,\ S = 0.3,\ \gamma_2 = 0.5, \gamma_1 = 0.5, Pe_b = 1.0, N_d = 0.5$

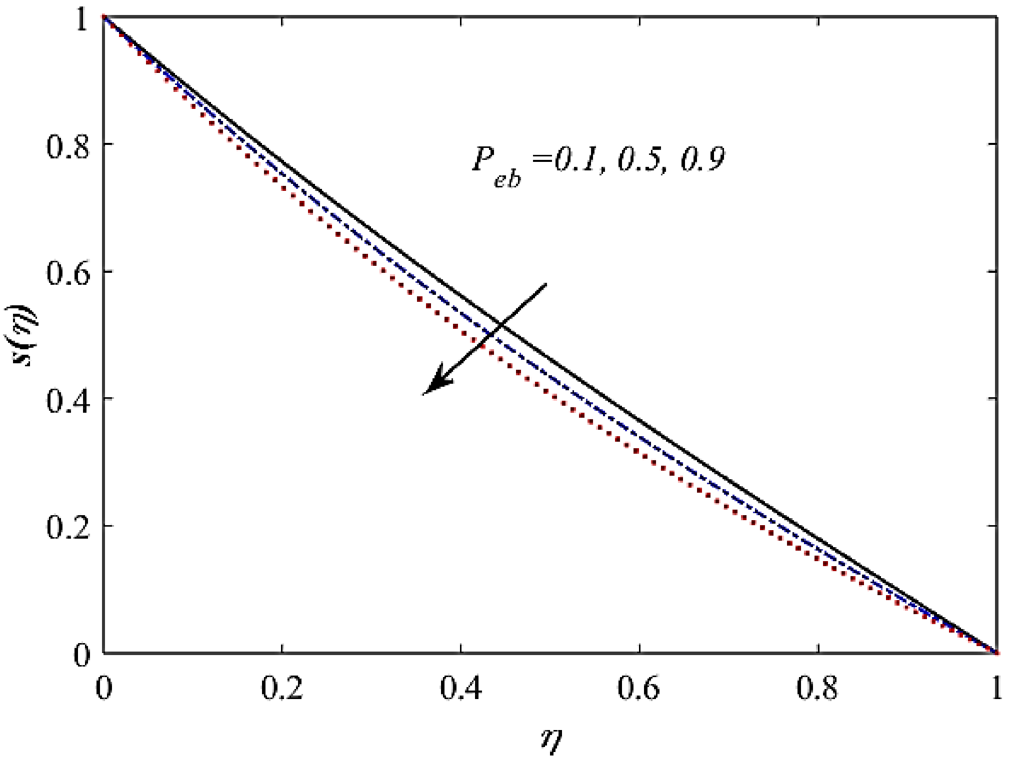

Figure 11. $s(\eta)$ against η for different Pe_b values. Here:
$P_r = 1.0,\ N_t = 0.3,\ N_b = 0.3,\ L_e = 0.2,\ S_q = 0.5,\ S = 0.3,\ \gamma_2 = 0.5,\ \gamma_1 = 0.5, N_d = 0.5, S_c = 1.0, M = 0.5.$

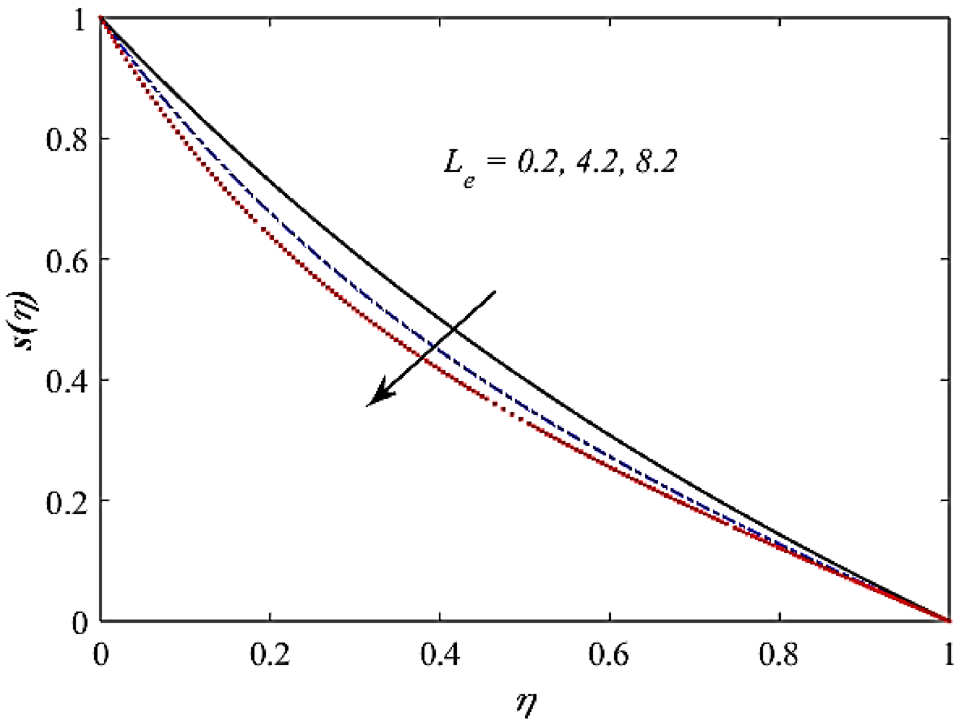

Figure 12. $s(\eta)$ against η for different L_e values. Here:
$M = 0.5,\ P_r = 1.0,\ N_t = 0.3,\ N_b = 0.3,\ S_q = 0.5,\ S = 0.3,\ \gamma_2 = 0.5,\ \gamma_1 = 0.5, N_d = 0.5, S_c = 1.0, Pe_b = 1.0$

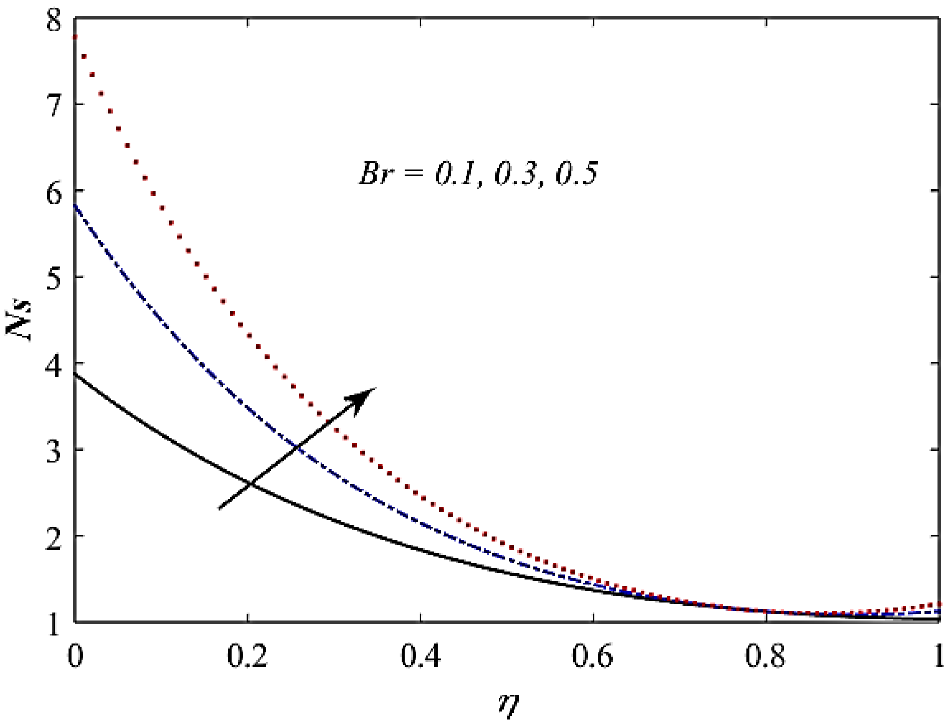

Figure 13. Impact of Brinkman number upon N_s. Here:
$M=0.5,\ P_r=1.0,\ N_b=N_t=0.3,\ L_e=0.2,\ S_q=0.5,\ S=0.3,\ \gamma_1=0.5,\ \gamma_2=0.5,\ \lambda=0.2,\ \Omega_c=0.5,$
$\Omega_T=1.0, S_c=1.0, Pe_b=1.0, N_d=0.5$

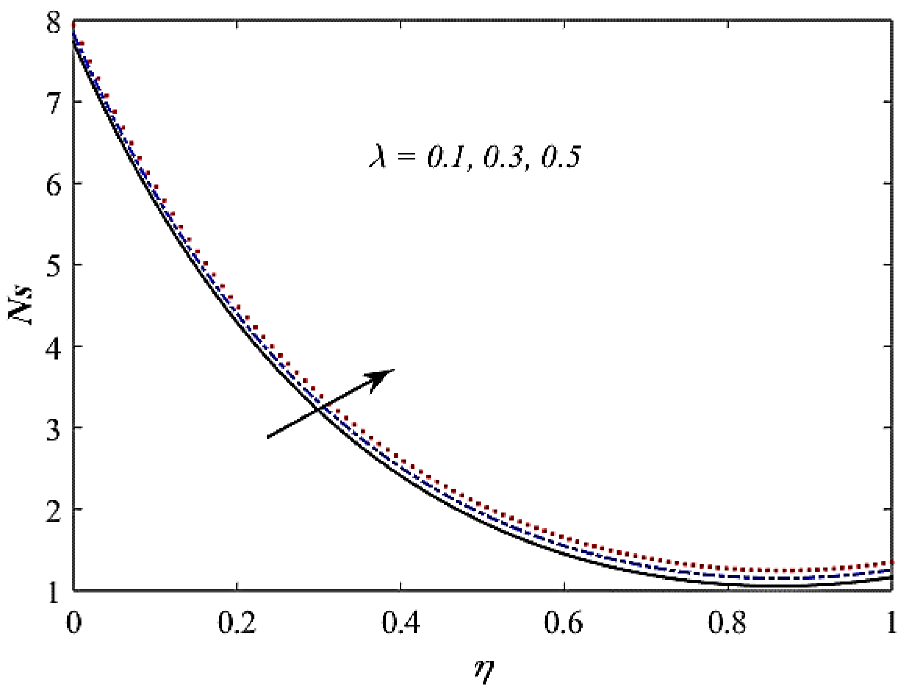

Figure 14. N_s against η for different λ values. Here:
$M=0.5,\ P_r=1.0,\ N_b=N_t=0.3,\ L_e=0.2,\ S_q=0.5,\ S=0.3,\ \gamma_1=0.5,\ \gamma_2=0.5,\ Br=0.5,\ \Omega_c=0.5,$
$\Omega_T=1.0, S_c=1.0, Pe_b=1.0, N_d=0.5, \varepsilon=0.5$

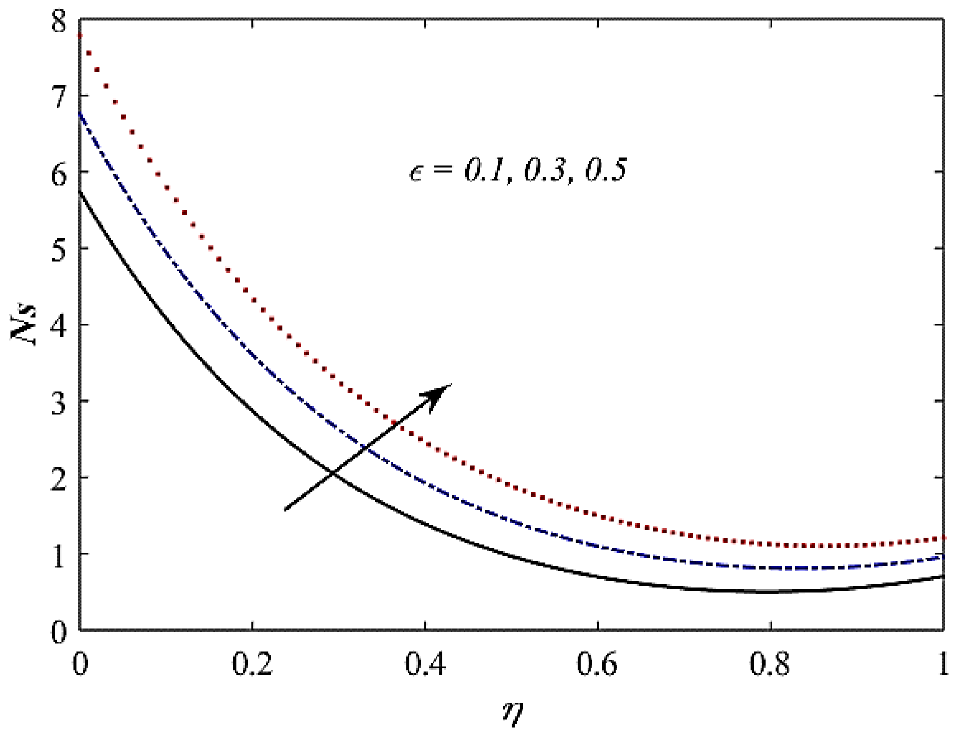

Figure 15. N_s profile for different ε values. Here:
$\lambda = 0.2,\ P_r = 1.0,\ N_b = N_t = 0.3,\ L_e = 0.2,\ S_q = 0.5,\ S = 0.3,\ \gamma_1 = 0.5,\ \gamma_2 = 0.5,\ Br = 0.5,\ \Omega_c = 0.5,$
$\Omega_T = 1.0, S_c = 1.0, Pe_b = 1.0, N_d = 0.5, \varepsilon = 0.5$

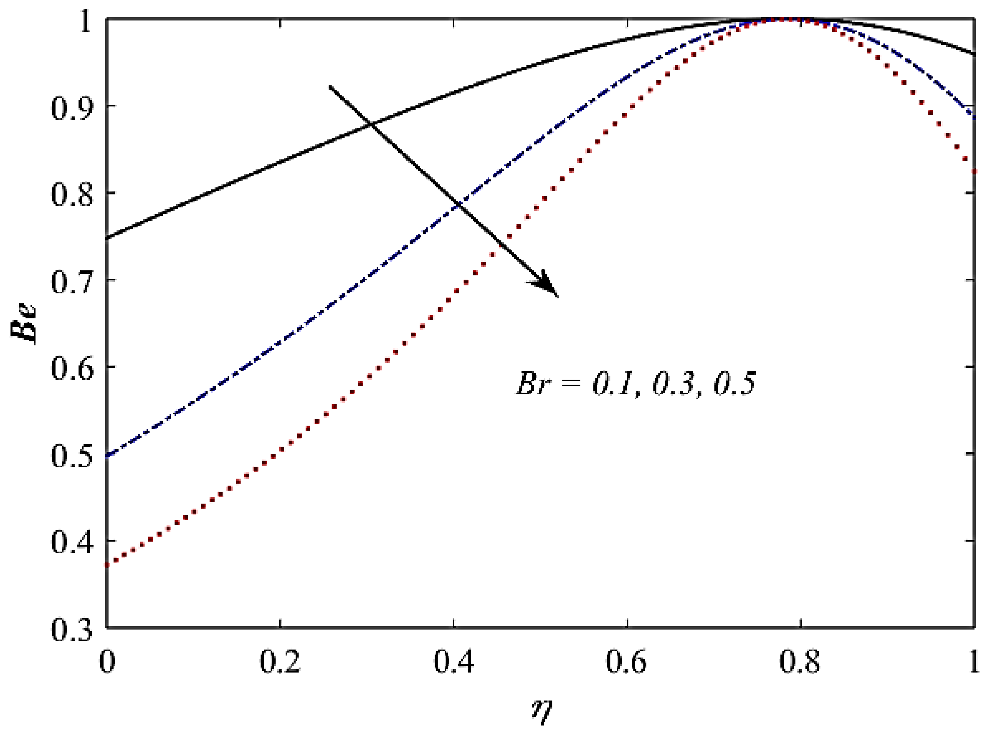

Figure 16. Be against η for different Br. Here:
$M = 0.5,\ P_r = 1.0,\ N_b = N_t = 0.3,\ L_e = 0.2,\ S_q = 0.5,\ S = 0.3,\ \gamma_1 = 0.5,\ \gamma_2 = 0.5,\ \lambda = 0.2,\ \Omega_c = 0.5,$
$\Omega_T = 1.0, S_c = 1.0, Pe_b = 1.0, N_d = 0.5, \varepsilon = 0.5$

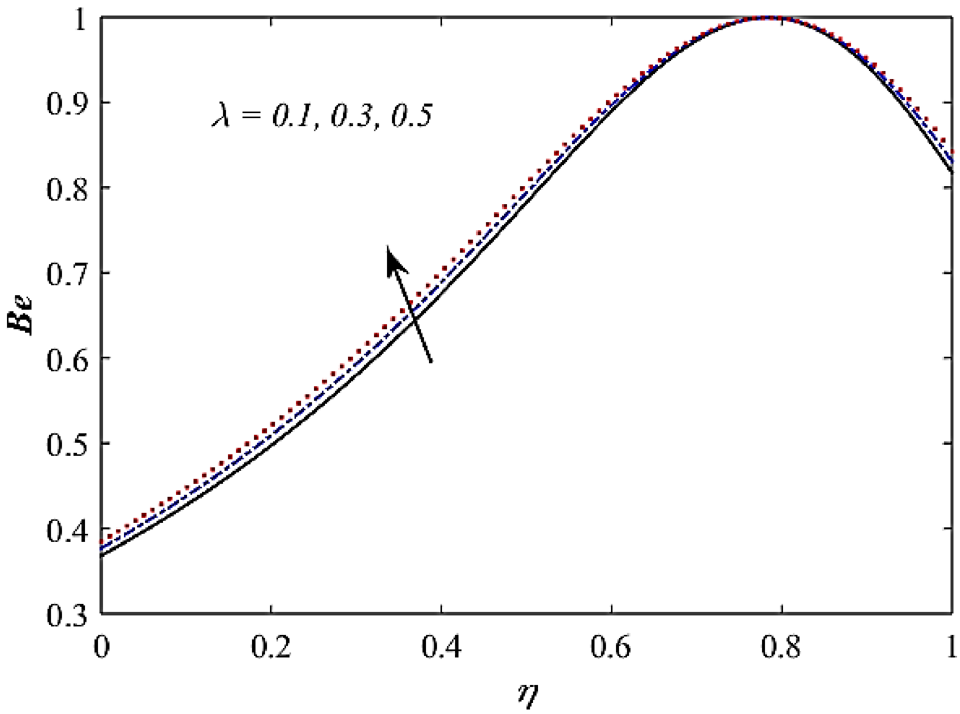

Figure 17. Be against η for different λ values. Here:
$M = 0.5,\ P_r = 1.0,\ N_b = 0.3,\ L_e = 0.2,\ S_q = 0.5,\ S = 0.3,\ \gamma_1 = 0.5,\ \gamma_2 = 0.5,\ Br = 0.5,\ \Omega_c = 0.5,$
$\Omega_T = 1.0, S_c = 1.0, Pe_b = 1.0, N_d = 0.5, N_t = 0.3, \varepsilon = 0.5$

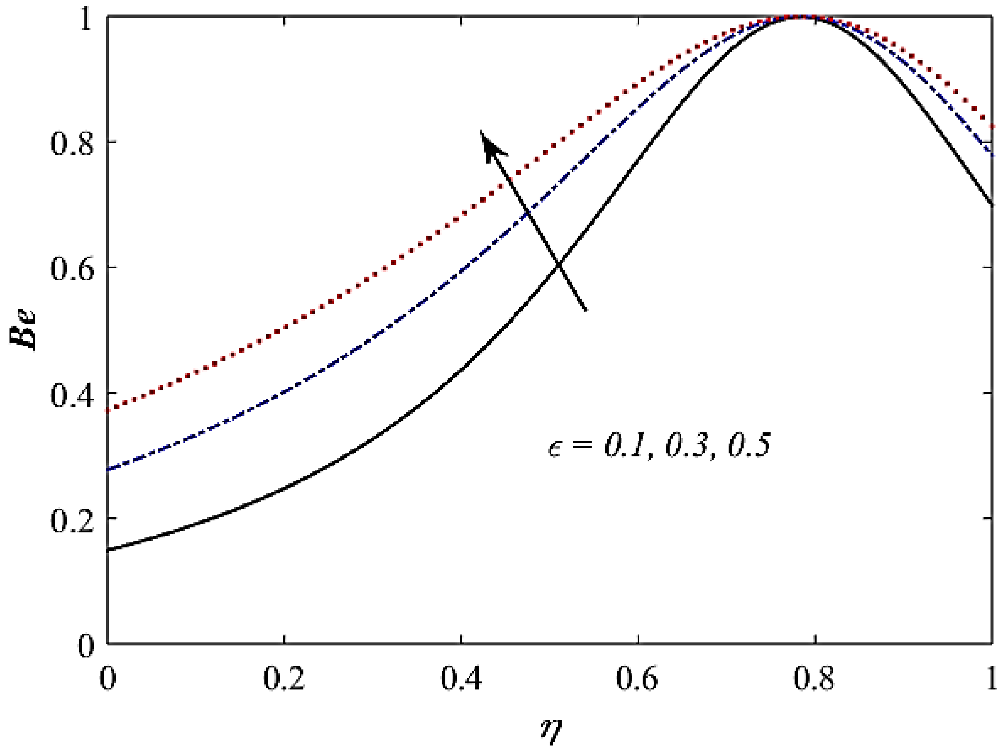

Figure 18. Be against η for different ε values. Here $\varepsilon = 0.5$
$M = 0.5,\ P_r = 1.0,\ N_t = 0.3,\ L_e = 0.2,\ S_q = 0.5,\ S = 0.3,\ \gamma_1 = 0.5,\ \gamma_2 = 0.5,\ Br = 0.5,\ \Omega_c = 0.5,$
$\Omega_T = 1.0, S_c = 1.0, Pe_b = 1.0, N_d = 0.5, N_b = 0.3, \varepsilon = 0.5$

Table 1. Comparison of $f''(1)$ with [34] at upper disk against different values of M , S_q and S .

M	S_q	S	**Present solution** $f''(1)$	**Previous solution** $f''(1)$
0.0	0.1	0.1	–2.40788	–2.40788
0.1			–2.40796	–2.40828
0.2			–2.40820	–2.40948
0.4			–2.40916	–2.41426
0.6			–2.41075	–2.42221
0.2	0.0	0.1	–2.40000	–2.40160
	0.2		–2.41640	–2.41735
	0.3		–2.42458	–2.42522
	0.4		–2.43276	–2.43308
	0.5		–2.44093	–2.44093
0.2	0.1	–0.1	–3.62115	–3.62306
		0.0	–3.01394	–3.01553
		0.1	–2.40820	–2.40948
		0.3	–1.20116	–1.20180
		0.4	–0.59984	–0.60016

Table 2. Skin friction coefficient $Cf_{0r} = f''(0)$ and $Cf_{1r} = f''(1)$ at lower and upper disks, respectively, for distinct M , S_q and S values, while the remaining parameters are taken as $P_r = 1, N_t = 0.3,$ $L_e = 0.2, \gamma_1 = 0.5, \gamma_2 = 0.5, Br = 0.5, \Omega_c = 0.5, \Omega_T = 1.0, S_c = 1.0, Pe_b = 1.0, N_d = 0.5, N_b = 0.3, \varepsilon = 0.5$

M	S_q	S	$Cf_{0r}(0)$	$Cf_{1r}(1)$
0.0	0.5	0.3	–3.05796	0.663548
1.0			–3.16659	0.616706
2.0			–3.47619	0.486557
0.5	0.5	0.3	–3.08539	0.651660
	1		–3.37119	0.518629
	1.5		–3.65676	0.398830
0.5	0.5	0.0	–1.14270	–1.14079
		0.2	–2.42474	0.061079
		0.4	–3.75952	1.235410

Table 3. Nusselt number $Nu_{0r} = -\theta'(0)$ and $Nu_{1r} = -\theta'(1)$ at lower and upper disks, respectively, for some P_r, S and γ_1 values. While rest of the parameters are considered as: $N_t = 0.3,\ \gamma_2 = 0.5,\ Br = 0.5,$ $\Omega_c = 0.5, \Omega_T = 1.0, S_c = 1.0, Pe_b = 1.0, N_d = 0.5, N_b = 0.3, \varepsilon = 0.5, M = 0.5, S_q = 0.5$

P_r	S	γ_1	$-\theta'(0)$	$-\theta'(1)$
1.0	0.3	0.5	0.489726	0.525109
2.0			0.479151	0.550872
3.0			0.468293	0.577253
3.0	0.0	0.5	0.347721	0.670680
	0.2		0.425792	0.609017
	0.4		0.512857	0.545118
3.0	0.3	0.0	0.745564	1.533170
		0.4	0.508439	0.660553
		0.8	0.377256	0.417748

Table 4. Sherwood number $Sh_{0r} = -\varphi^{'}(0)$ and $Sh_{1r} = -\varphi^{'}(1)$ at upper and lower disks, respectively, for different P_r, L_e, S and γ_2 values. While the other parameters considered as: $N_t = 0.3,\ \gamma_1 = 0.5,$ $Br = 0.5,\ \Omega_c = 0.5, \Omega_T = 1.0, S_c = 1.0, Pe_b = 1.0, N_d = 0.5, N_b = 0.3, \varepsilon = 0.5, M = 0.5, S_q = 0.5$

P_r	L_e	S	γ_2	$-\varphi^{'}(0)$	$-\varphi^{'}(1)$
1.0	0.2	0.3	0.5	0.523655	0.464681
2.0				0.534558	0.438689
3.0				0.545747	0.412077
3.0	0.2	0.3	0.5	0.545747	0.412077
	0.6			0.574204	0.392818
	1.0			0.602960	0.373865
3.0	0.2	0.0	0.5	0.656549	0.325293
		0.2		0.585130	0.382497
		0.4		0.504182	0.442043
3.0	0.2	0.3	0.0	1.133810	0.760669
			0.4	0.612346	0.451357
			0.8	0.406911	0.330212

CONCLUSIONS

This study investigates the entropy effects in the unsteady squeezing bioconvection flow of nanofluid between a pair of disks arranged in parallel. The disk at bottom is subjected to suction, and stretched horizontally, while the disk at the upper end moves vertically, creating a squeezing effect. Slip conditions are applied for temperature and concentration. The problem is normalized using similarity transformations, and numerical solution is acquired using the bvp4c. The study yields the following principal outcomes:

- The profile $f^{'}(\eta)$ is enhanced near the upper disk and decreased near the lower disk when the squeezing parameter S_q and magnetic parameter M are amplified.
- A decrease in the fluid velocity is caused as the suction parameter is increased.
- Suction parameter S results in a drop in the fluid velocity.
- The Brownian motion and thermophoresis parameters serve as a vital function in modifying the temperature and concentration fields, influencing particle behavior and thermal conductivity.
- The Schmidt number S_c and bioconvection Peclet number Pe_b affect the distribution of gyrotactic microorganisms, higher Schmidt numbers result in lower microorganism concentration due to reduced mass diffusivity.
- Entropy generation increases with higher Brinkman numbers, diffusion parameters, and microorganism diffusivity, indicating a decrease in thermal system’s efficiency.
- The Bejan number is influenced by nanoparticle and microorganism diffusion, showing the relationship between heat transfer and viscous dissipation in the system.

The findings offer insights for optimizing nanofluid-based systems, improving thermal and bioconvection processes, and enhance the efficiency of engineering and environmental applications.

REFERENCES

1. Stefan J. Versuche über die scheinbare Adhäsion. Sitzungsberichte der Kaiserlichen Akademie der Wissenschaften, Mathematisch-Naturwissenschaftliche Classe. 1874;69:713–735.
2. Misyura V. Laminar flow of an incompressible liquid between two rotating discs. Fluid Dyn. 1972;7(5):860–4.
3. Batista M. Steady flow of incompressible fluid between two co-rotating disks. Appl Math Model. 2011;35(10):5225–33.

4. Tashtoush B, Tahat M, Probert D. Heat transfers and radial flows via a viscous fluid squeezed between two parallel disks. Appl Energy. 2001;68(3):275–88.
5. Khan SI, Ahmed N, Khan U, Jan SU, Mohyud-Din S. Heat transfer analysis for squeezing flow between parallel disks. J Egypt Math Soc. 2015;23(2):445–50.
6. Duwairi H, Tashtoush B, Damseh RA. On heat transfer effects of a viscous fluid squeezed and extruded between two parallel plates. Heat Mass Transf. 2004;41:112–7.
7. Khaled AR, Vafai K. Hydromagnetic squeezed flow and heat transfer over a sensor surface. Int J Eng Sci. 2004;42(5–6):509–19.
8. Choi SU, Eastman JA. Enhancing thermal conductivity of fluids with nanoparticles. Argonne National Lab (ANL); 1995.
9. Hashim M, Khan M, Hamid A. Convective heat transfer during the flow of Williamson nanofluid with thermal radiation and magnetic effects. Eur Phys J Plus. 2019;134:1–12.
10. Benos LT, Karvelas E, Sarris I. A theoretical model for the magnetohydrodynamic natural convection of a CNT-water nanofluid incorporating a renovated Hamilton-Crosser model. Int J Heat Mass Transf. 2019;135:548–60.
11. Kumar R, Bhattacharyya A, Seth G, Chamkha AJ. Transportation of magnetite nanofluid flow and heat transfer over a rotating porous disk with Arrhenius activation energy: Fourth order Noumerov's method. Chin J Phys. 2021;69:172–85.
12. Ullah MZ, Jang T. An efficient numerical scheme for analyzing bioconvection in von-Kármán flow of third-grade nanofluid with motile microorganisms. Alex Eng J. 2020;59(4):2739–52.
13. Sk MT, Das K, Kundu PK. Multiple slip effects on bioconvection of nanofluid flow containing gyrotactic microorganisms and nanoparticles. J Mol Liq. 2016;220:518–26.
14. Xu H. Modelling unsteady mixed convection of a nanofluid suspended with multiple kinds of nanoparticles between two rotating disks by generalized hybrid model. Int Commun Heat Mass Transf. 2019;108:104275.
15. Qayyum S, Imtiaz M, Alsaedi A, Hayat T. Analysis of radiation in a suspension of nanoparticles and gyrotactic microorganism for rotating disk of variable thickness. Chin J Phys. 2018;56(5):2404–23.
16. Alshomrani AS, Ullah MZ, Baleanu D. Importance of multiple slips on bioconvection flow of cross nanofluid past a wedge with gyrotactic motile microorganisms. Case Stud Therm Eng. 2020;22:100798.
17. Bejan A. Entropy generation through heat and fluid flow. New York: Wiley; 1982.
18. Oztop HF, Al-Salem K. A review on entropy generation in natural and mixed convection heat transfer for energy systems. Renew Sustain Energy Rev. 2012;16(1):911–20.
19. Aïboud S, Saouli S. Entropy analysis for viscoelastic magnetohydrodynamic flow over a stretching surface. Int J Non Linear Mech. 2010;45(5):482–9.
20. Sahin AZ, Yilbas BS. Entropy generation in the flow system generated in between two parallel plates due to bivertical motion of the top plate. Sadhana. 2009;34:455–66.
21. Rajvanshi S, Saini B, VVASU S. MHD squeezing flow between two parallel plates. Heat Transf. 2013;12(2):181–98.
22. Murshid N, Mulki H, Abu-Samha M, Owhaib W, Raju SS, Raju CS, et al. Entropy generation and statistical analysis of MHD hybrid nanofluid unsteady squeezing flow between two parallel rotating plates with activation energy. Nanomaterials. 2022;12(14):2381.
23. Butt AS, Ali A. Analysis of entropy generation effects in unsteady squeezing flow in a rotating channel with lower stretching permeable wall. J Taiwan Inst Chem Eng. 2015;48:8–17.
24. Rashidi M, Ali M, Freidoonimehr N, Nazari F. Parametric analysis and optimization of entropy generation in unsteady MHD flow over a stretching rotating disk using artificial neural network and particle swarm optimization algorithm. Energy. 2013;55:497–510.
25. Louati H, Khan S, Mansoor M, Hilali SO, Gargouri A. Analysis of entropy generation via non-similar numerical approach for magnetohydrodynamics Casson fluid flow with Joule heating. Entropy. 2024;26(8):702.
26. Waqas H, Khan SU, Hassan M, Bhatti M, Imran M. Analysis on the bioconvection flow of modified second-grade nanofluid containing gyrotactic microorganisms and nanoparticles. J Mol Liq. 2019;291:111231.

27. Wu Y, Chaudhry M, Maqbool N, Tahir M, Basit MA, Imran M. Entropy generation in radiative motion of tangent hyperbolic nanofluid in the presence of gyrotactic microorganisms and activation energy. Front Phys. 2024;12:1409318.
28. Khan NS, Shah Q, Bhaumik A, Kumam P, Thounthong P, Amiri I. Entropy generation in bioconvection nanofluid flow between two stretchable rotating disks. Sci Rep. 2020;10(1):4448.
29. Zuhra S, Khan NS, Islam S. Magnetohydrodynamic second-grade nanofluid flow containing nanoparticles and gyrotactic microorganisms. Comput Appl Math. 2018;37:6332–58.
30. Hussain T, Xu H. Time-dependent squeezing bio-thermal MHD convection flow of a micropolar nanofluid between two parallel disks with multiple slip effects. Case Stud Therm Eng. 2022;31:101850.
31. Hashmi MMM, Hayat T, Alsaedi A. On the analytic solutions for squeezing flow of nanofluid between parallel disks. Nonlinear Anal Model Control. 2012;17(4):418–30.
32. Pradhan S, Baag S, Mishra S, Acharya M. Squeezing flow analysis of MHD micropolar fluid on radial and angular velocity: A semianalytical approach. Heat Transf Asian Res. 2019;48(7):2799–818.
33. Keskin AÜ, Keskin AÜ. Solution of BVPs using bvp4c and bvp5c of MATLAB. Boundary value problems for engineers: With MATLAB solutions. 2019;417–510.
34. Hayat T, Yousaf A, Mustafa M, Asghar S. Influence of heat transfer in the squeezing flow between parallel disks. Chem Eng Commun. 2012;199(8):1044–62.
35. Wu Y, Chaudhry M, Maqbool N, Tahir M, Basit MA, Imran M. Entropy generation in radiative motion of tangent hyperbolic nanofluid in the presence of gyrotactic microorganisms and activation energy. Frontiers in Physics. 2024 Oct 25;12:1409318.
36. Khan NS, Shah Q, Bhaumik A, Kumam P, Thounthong P, Amiri I. Entropy generation in bioconvection nanofluid flow between two stretchable rotating disks. Scientific Reports. 2020 Mar 10;10(1):4448.
37. Zuhra S, Khan NS, Islam S. Magnetohydrodynamic second-grade nanofluid flow containing nanoparticles and gyrotactic microorganisms. Computational and Applied Mathematics. 2018 Nov;37(5):6332-58.
38. Hussain T, Xu H. Time-dependent squeezing bio-thermal MHD convection flow of a micropolar nanofluid between two parallel disks with multiple slip effects. Case Studies in Thermal Engineering. 2022 Mar 1;31:101850.
39. Hashmi MM, Hayat T, Alsaedi A. On the analytic solutions for squeezing flow of nanofluid between parallel disks. Nonlinear Analysis: Modelling and Control. 2012 Oct 25;17(4):418-30.
40. Pradhan SR, Baag S, Mishra SR, Acharya MR. Squeezing flow analysis of MHD micropolar fluid on radial and angular velocity: A semianalytical approach. Heat Transfer—Asian Research. 2019 Nov;48(7):2799-818.
41. Keskin AÜ. Solution of BVPs using bvp4c and bvp5c of MATLAB. InBoundary value problems for engineers: with MATLAB solutions 2019 Jun 20 (pp. 417-510). Cham: Springer International Publishing.
42. Hayat T, Yousaf A, Mustafa M, Asghar S. Influence of heat transfer in the squeezing flow between parallel disks. Chemical Engineering Communications. 2012 Aug 1;199(8):1044-62.

